A model of the dilution of a forced two-phase chemical plume in a horizontal wind

M. Epstein, H. K. Fauske and G. M. Hauser
Fauske & Associates, Inc., 16W070 West 83rd Street, Burr Ridge, IL 60521, USA

Accidental releases of volatile liquid chemicals from pressurized storage vessels result in the formation of high-momentum flashed jets with liquid phases comprised of extremely fine droplets (aerosol). These jets are typically heavier than air. The subject of this paper is the description of a turbulent entrainment model that predicts the trajectory and dilution of such releases when the release point is elevated above ground-level in a horizontal wind. The model is compared with available field test data for pressurized liquid releases and is found to describe the observations to a degree of accuracy adequate for most hazard assessment purposes. The comparisons include the field measurements made during the liquid ammonia (NH_3) and liquid hydrofluoric acid (HF) release test series, namely Desert Tortoise and Goldfish respectively, at the US Department of Energy Fuels Test Facility. The model indicates that over the 3000 m distance in which measurements were made, there is no need to invoke atmospheric turbulence to explain the dilution of the ammonia jet. However, atmospheric turbulence is predicted to dominate the mixing in the far field of the weaker HF jet.

(Keywords: release; modelling; wind speed)

Increased recognition that most emergency releases from chemical storage or process vessels involve the escape of volatile, pressurized liquids has led to a need for predictive models of two-phase liquid–vapour forced plumes (jets). Releases of liquids from pressurized vessels have high momentum. A rapid depressurization and expansion occurs just outside the release orifice. During depressurization the liquid jet material is converted into aerosol as a result of flashing to vapour. Following external expansion to atmospheric pressure, turbulent mixing of the jet with the atmosphere occurs and the surrounding air and water vapour are entrained into the jet at a rate proportional to the mean jet velocity[1].

The temperature of the jet decreases with distance from the release point, owing to the evaporation of the jet aerosol by the entrained, relatively warm air. As a result the water vapour in the entrained air may condense to a fog. The observed persistence of visible aerosol plumes produced by the release of volatile liquids is probably due to condensation of the atmospheric water content. Beyond some not very significant distance from the release point (source) both liquid phases, jet material and water, are consumed by evaporation and the forced plume behaviour is one of an all-gas heavier-than-air release. As dilution continues and the jet slows down, it begins to spread over the ground under the influence of gravity and loses its roughly circular shape. As demonstrated later, in this intermediate jet slumping (or gravity current) phase the rate of entrainment of air is still proportional to the mean jet flow velocity, with the proportionality factor taken to be a constant. In the final phase of jet behaviour, far from the release point, the atmosphere eddies determine jet dilution behaviour.

The SLAB[2], FEM3[3], and DEGADIS[4] models were developed to model the dispersion of ground-level plumes of heavy gases released into the atmosphere. They have recently been modified to account for the presence of a liquid phase[5–7]. These models, however, lack treatments of one or more of the following phenomena that are of importance in understanding and quantifying the behaviour of two-phase high momentum releases: external depressurization close to the source, condensation of entrained atmospheric humidity, entrainment of the ambient by the jet's self-generated turbulence, and the motion of the two-phase jet when released above ground level at perhaps some non-zero angle from the horizontal.

A theory for the spreading of a steady-state initially high-momentum two-phase jet in a horizontal wind is proposed here, in which it is assumed that for some rather large distance downwind of the release location (in some cases of the order of thousands of metres), the effects of buoyancy and/or atmospheric turbulence on the inflow or entrainment velocity may be ignored in comparison with the effects of turbulence generated by the jet. This assumption is what distinguishes the present work from most of the previous modelling efforts, which are based on the notion that the rate of engulfment of air by the jet is determined by

Received 22 September 1989; revised 16 October 1989

0950–4230/90/030280–11

the atmospheric boundary layer and/or by gravity beginning at relatively small distances from the source. In the present model only two distinct phases of jet entrainment behaviour are considered: mixing by the jet's self-generated turbulence in the near field and mixing by environmental turbulence in the far field. Moreover a fairly sharp transition point at which near-field entrainment behaviour changes to far-field behaviour is assumed. The intermediate phase involving the inhibiting effect of buoyancy on mixing into the jet is regarded as insignificant.

In developing the two-phase jet dispersion model, it is convenient to divide the jet into three regions: the depressurization zone where aerosol formation takes place, a two-dimensional 'jet trajectory zone' for above ground-level releases, and a ground-level jet behaviour zone beyond the distance to plume 'touchdown'. The depressurization zone is treated with a standard liquid flash and momentum balance equation, as discussed by Fauske and Epstein[8]. The trajectory and dilution of the jet in the intermediate, elevated jet zone is predicted with a two-phase version of the buoyant jet entrainment models that were originally developed for smoke stack or cooling water discharge plumes (see Gebhart *et al.*[9]). Finally, the ground level dispersion process, which includes gravity-driven lateral spreading as well as turbulent entrainment of air and water vapour, is approached with a steady-state version of the SLAB entrainment model[2], modified to include two-phase flow effects.

Analysis

A schematic representation of the high-momentum two-phase plume is shown in *Figure 1*. The jet is inclined and released above ground level. The jet passes through several physical regimes along its path. The regimes are modelled separately in the following sections.

Zone of depressurization

In this region the jet undergoes a rapid depressurization to or slightly below ambient pressure within a distance from the release orifice of approximately two orifice diameters. It is within this zone that the liquid disintegrates into fine droplets in the 10–50μm size range. The jet expansion in this region is rapid and due almost entirely to vapour production; its interaction with the atmosphere is negligible and very little mixing between jet and ambient occurs. Thus friction, heat and momentum exchange with the ambient environment at pressure P_∞ are assumed to be negligible.

In an emergency release situation, liquid at high pressure usually escapes from a vessel whose stagnation condition is subcooled and exit choked mass flux well-represented by

$$G = C_D\sqrt{2[P_0 - P_{j,s}(T_0)]\rho_{j,f}} \quad (1)$$

where P_0 is the stagnation pressure; $P_{j,s}(T_0)$ is the vapour (or saturation) pressure of the escaping jet material corresponding to the liquid stagnation temperature T_0; and $\rho_{j,f}$ is the density of the jet material's liquid phase. This Bernoulli type expression shows reasonable agreement in experimental comparisons.

A spacewise calculation of two-dimensional (or axisymmetric) jet pressure and velocity profiles is difficult. However, it is possible to estimate the fully expanded jet properties at the end of the depressurization zone, when the jet pressure everywhere has approached the ambient pressure. High pressure

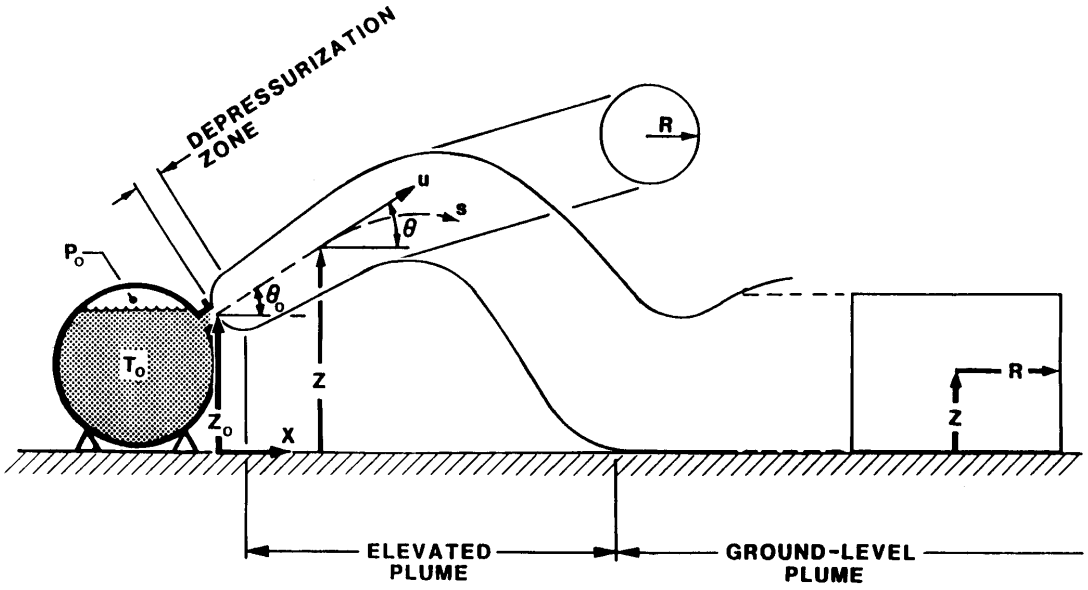

Figure 1 Flow regimes of a high-momentum two-phase release and the coordinate system

flashing liquids produce extremely fine droplets, so that phase velocities and temperatures are quickly equalized. The principle of conservation of momentum flux applied to this homogeneous mixture provides a simple relation between the fully expanded jet velocity u_e at the end of the depressurization zone and the break (or choke) plane quantities

$$u_e = \frac{G}{\rho_{j,f}} + \frac{P_{j,s}(T_0) - P_\infty}{G} \tag{2}$$

To obtain the quality of the fully expanded jet, x_e, we invoke the condition of constant stagnation enthalpy*:

$$h_o = h_{j,f,s}(P_\infty) + x_e h_{j,fg}(P_\infty) \tag{3}$$

The kinetic energy of the two-phase jet is notably quite low (relative to that of an all-gas sonic discharge) and therefore is not included in the above equation. For the all-liquid discharge considered here, Equation (3) becomes

$$x_e = \frac{c_{j,f}[T_0 - T_{j,s}(P_\infty)]}{h_{j,fg}} \tag{4}$$

The area of the depressurized jet A_e is related to the area of the break A_b through the equation for the conservation of mass:

$$A_e = \frac{A_b G}{u_e \rho_e}$$

in which the expanded jet density, ρ_e, is given by the definition

$$\rho_e = \left[\frac{x_e}{\rho_{j,g,s}(P_\infty)} + \frac{1 - x_e}{\rho_{j,f,s}(P_\infty)}\right]^{-1} \tag{5}$$

The volume occupied by the liquid at the end of the depressurization zone can readily be shown to be negligible. Thus the equilibrium quantity $\rho_{j,g,s}(P_\infty)$ can be identified with the mass of the vapour per unit spatial volume, i.e.

$$\rho_{j,g,e} = \rho_{j,g,s}(P_\infty) \tag{6}$$

The mass of the liquid phase with respect to the same spatial volume is given by

$$\rho_{j,f,e} = (1 - x_e)\,\rho_e \tag{7}$$

The quantities u_e, A_e, $\rho_{j,g,e}$, and $\rho_{j,f,e}$ are used as input to the jet trajectory and dilution model.

Airborne jet trajectory zone

This zone begins when the jet is depressurized to atmospheric pressure. The forced plume (jet) is not necessarily released at ground level and the component of initial jet velocity, u_e, is not necessarily parallel to the horizontal ambient flow (wind), but may be inclined away from it, horizontally. Thus near the rupture opening (or vent) the solution of the equations of motion may require that the jet rise. However, further downstream the heavier-than-air jet is influenced by the gravitational field and its trajectory is similar in shape to that of a projectile (see *Figure 1*). The trajectory 'zone' or, equivalently, the flight of the jet terminates upon contact with the ground.

The equations are written to take account of a steady, horizontal, wind. The wind direction or velocity, W, does not change with altitude z, the jet lying in the x, z plane (see *Figure 1*). The mean velocity inside the jet is denoted by the symbol u. The centreline of the jet makes an angle θ with the horizontal, s is the distance along the jet, A is the cross-sectional area of the jet, and C is the perimeter of the cross-section. For simplicity, we assume that inside the jet the velocity, vapour and liquid concentrations, and temperature are uniform in the crosswind plane. Over the distance the jet is airborne its cross-section is taken to be circular and its radius R is assumed to be small compared with the centreline radius of curvature (slender plume approximation).

Once the jet is depressurized to atmospheric pressure, the jet expands solely by entrainment of ambient air. The principal assumption of this theory is that, for some significant distance from the source, the effects of atmospheric turbulence may be ignored, provided the initial momentum of the jet is high enough. Hirst[10] performed an analysis on a limited set of experimental data on buoyant jet flow discharged into a uniform cross stream to determine the jet entrainment velocity due to the jet's self-generated turbulence. Using the form suggested by Morton *et al.*[1] as a basis, he constructed a correlation for the entrainment velocity v_{en}. For jets with a two-dimensional trajectory, his expression becomes

$$v_{en} = \left(\frac{\rho}{\rho_\infty}\right)^{1/2} (E_0|u - W\cos\theta| + E_1 W|\sin\theta|) \tag{8}$$

where the term $|u - W\cos\theta|$ represents the relative velocity of the jet with respect to the wind. Actually, Equation (8) is a combination of the entrainment model proposed by Hirst and the entrainment model of Ricou and Spalding[11] for vastly different jet and ambient densities, ρ and ρ_∞, respectively. Precise definitions of ρ and ρ_∞ are given below. Equation (8) reduces to the entrainment function of Hirst in the limit $\rho \to \rho_\infty$. The constants of proportionality E_0 and E_1 are called the entrainment coefficients. Ricou and Spalding[11] have verified through measurements that for pure momentum jets ($E_1 = 0$) values of E_0 lie within the range 0.06 to 0.12.

Morton[12] found that if a uniform velocity profile is used $E_0 = 0.12$ results in the best agreement between theory and experiment. From data on buoyant water jets discharged at varying angles into flowing aqueous salt solutions, Hirst[10] specified the values $E_0 = 0.057$ and $E_1 = 0.513$. His value of E_0 is consistent with the lower end of the range recommended by Ricou and Spalding for pure momentum jets ($E_1 = 0$). Hoult *et al.*[13] suggested, also on the basis of experiments with salt solutions and water, $E_0 = 0.12$ and $E_1 = 0.6$. Their E_0 is in agreement with the upper end of the range 0.06 to 0.12. In the calculations which follow, we shall adopt Equation (8) and use values of E_0 and E_1 of 0.1 and

*The reader should refer to the Nomenclature for the meanings of the symbols and subscripts

0.5, respectively. The jet trajectory can now be determined from the conservation equations for mass, momentum and energy, using the entrainment equation to determine the rate of mass, momentum and energy addition into the jet.

The equations for the conservation of mass of the discharge material, air, and the atmospheric water content are

$$\frac{d}{ds}[(\rho_{j,g} + \rho_{j,f})uA] = 0 \tag{9}$$

$$\frac{d}{ds}(\rho_a uA) = \rho_{a,\infty} v_{en} C \tag{10}$$

$$\frac{d}{ds}[(\rho_{w,g} + \rho_{w,f})uA] = \rho_{w,g,\infty} v_{en} C \tag{11}$$

Note that in addition to the liquid aerosol of the discharge jet material we allow for the possibility of water droplet formation via condensation of the entrained water vapour within the cold jet (see Equation (11)). Neglecting the volume occupied by the jet aerosol and water droplets, we can express the overall spatial density, ρ, of the three component two-phase mixture as the sum of the spatial densities of the components:

$$\rho = \rho_{j,g} + \rho_{j,f} + \rho_a + \rho_{w,g} + \rho_{w,f} \tag{12}$$

The momentum equation in the vertical direction is a balance between plume momentum and mass:

$$\frac{d}{ds}(\rho A u^2 \sin\theta) = -g(\rho - \rho_\infty)A \tag{13}$$

where ρ_∞ is the density of the air/water vapour atmosphere, namely

$$\rho_\infty = \rho_{a,\infty} + \rho_{w,g,\infty} \tag{14}$$

The momentum equation in the horizontal direction is a balance between jet momentum and momentum entrained:

$$\frac{d}{ds}(\rho A u^2 \cos\theta) = W\frac{d}{ds}(\rho A u) \tag{15}$$

Conservation of heat may be written in the following form:

$$\frac{d}{ds}(\rho u A h) = \rho_{a,\infty} v_{en} C h_{a,\infty} + \rho_{w,g,\infty} v_{en} C h_{w,g,\infty} \tag{16}$$

where h is the overall enthalpy of the mixture within the jet; it is given by the definition

$$\rho h = \rho_{j,g} h_{j,g} + \rho_{j,f} h_{j,f} + \rho_a h_a + \rho_{w,g} h_{w,g} + \rho_{w,f} h_{w,f} \tag{17}$$

The energy equation, Equation (16), may be readily converted from enthalpy to temperature as the dependent variable by introducing the thermodynamic relation $h(T)$ for each species, assuming the vapour phases are ideal and the liquid phases are incompressible. The height z of the jet above ground level is, in differential form,

$$\frac{dz}{ds} = \sin\theta \tag{18}$$

and the horizontal distance x from the rupture opening is given by

$$\frac{dx}{ds} = \cos\theta \tag{19}$$

Note that in writing the above equations, we have neglected the length of the depressurization zone. This length is typically quite small relative to the range of the jet. To predict the densities of the vapour phases in the presence of their condensed phases it is assumed that thermodynamic equilibrium is locally achieved within the jet. Thus, utilizing the ideal gas equation of state, we have

$$\rho_{j,g} = \frac{P_{j,s}(T)}{R_j T} \tag{20}$$

$$\rho_{w,g} = \frac{P_{w,s}(T)}{R_w T} \tag{21}$$

The pressure within the jet is equal to the atmospheric pressure P_∞. This requirement gives

$$P_\infty = \rho_{j,g} R_j T + \rho_{w,g} R_w T + \rho_a R_a T \tag{22}$$

Finally, since the cross-section of the jet is taken to be circular, the radius R, circumference and cross-sectional area are related by the expressions

$$C = 2\pi R = 2(\pi A)^{1/2} \tag{23}$$

The above equations express the mathematical formulation of the model and are sufficient to determine the nine coupled unknown quantities $\rho_{j,g}$, $\rho_{j,f}$, $\rho_{w,g}$, $\rho_{w,f}$, ρ_a, u, A, T and θ as a function of the coordinates x,z. These quantities are subject to the following initial conditions when $x = 0$ and $z = z_0$:

$$\rho_{j,g} = \rho_{j,g,e}, \rho_{j,f} = \rho_{j,f,e} \tag{24}$$

$$\rho_{w,g} = \rho_{w,f} = \rho_a = 0 \tag{25}$$

$$u = u_e, A = A_e \tag{26}$$

$$T = T_{j,s}, \theta = \theta_0 \tag{27}$$

The initial thermodynamic state of the mixture, at the end of the depressurization zone, is one of jet material aerosol in equilibrium with its vapour phase. Downwind of the release point humid air is entrained into the jet causing further evaporation of the liquid jet material. At first water exists within the jet only as vapour and Equation (11) is integrated with $\rho_{w,f} = 0$. As a result of a combination of the cooling of the jet by the evaporation of the released liquid jet material and the buildup in the water vapour concentration by entrainment of the surrounding air, the water vapour may become saturated so that both vapour and liquid water are present in the system. In some systems there is a tendency of jet material vapour to be soluble in liquid water. This effect is ignored in the present model. As the amount of air increases, the liquid water also begins to evaporate. Ultimately all the water and all the jet material are in vapour form. Usually the water is the last to evaporate. The evaporation of the water in the far field will tend to prolong the persistence of the cool jet beyond the distance to ground contact.

The zone of ground-level dispersion

This region begins at touchdown or, in mathematical terms, when the elevation of the centreline of the jet is equal to its radius (i.e. $z = R$, see *Figure 1*). The atmospheric dispersion of the ground-level jet is affected by both entrainment of the atmosphere and gravity spreading. Gravity spreading is driven primarily by the excess hydrostatic pressure caused by the density difference between the jet and the atmosphere.

In the initial phase of ground-level jet behaviour, the turbulent motion within the jet is normally still due to the movement of the jet itself and, accordingly, Equation (8) for v_{en} remains valid. Of course in the final phase of jet behaviour, far downwind of the source, the energy containing eddies of environmental turbulence dominate mixing and the ground-level jet growth is strictly due to the action of the wind. The far-field jet growth is assumed to be well-described by the Gaussian plume, point source solution to the atmospheric advection-diffusion equation. Accordingly, a realistic equation for the entrainment velocity in the far field is

$$v_{en} = \frac{\pi W}{C} \frac{d}{dx} [\sigma_y(x)\sigma_z(x)] \tag{28}$$

which when combined with the conservation of mass equation gives the point source Gaussian solution for the ground-level concentration of the released species in the far field of the jet. In the above equation, $\sigma_y(x)$ and $\sigma_z(x)$ are the dispersion coefficients (or standard deviations) for the crosswind plane. The most widely used σ_y and σ_z functions are the so-called Pasquill-Gifford curves[14]. These empirically determined functions depend on the atmospheric stability classes. The field observations reported by Burgess *et al.*[15] suggest that the dispersion of heavier-than-air ground-hugging vapours is best represented by Gaussian theory when σ_y and σ_z are based on the most stable atmospheric condition, stability class F, regardless of the actual state of the atmosphere. This recommendation is followed here.

Close to the source, the entrainment velocity given by Equation (8) greatly exceeds that given by Equation (28) and vice versa at distances far from the source. One would expect, therefore, a fairly definite transition point (or perhaps a short transition zone) at which the character of the jet changes when the near- and far-field entrainment velocities are comparable. Therefore, during the course of a calculation a switch is made from Equation (8) to Equation (28) at the location in which both equations predict the same entrainment velocity, thereby merging the high-momentum jet theory with the Gaussian plume model.

It is obvious that by equating the two entrainment velocity laws, Equations (8) and (28), the intermediate phase of jet behaviour involving buoyancy-dominated dispersion effects has been assumed to be insignificant. This assumption implies the dominancy of inertial force over the buoyancy force. The ratio of jet buoyancy to inertia is given by the Richardson number, defined by

$$\mathrm{Ri} = \frac{2g(\rho - \rho_\infty)z}{\rho u^2} \tag{29}$$

The work of Ellison and Turner[16] showed that the entrainment is not buoyancy dominated if $\mathrm{Ri} \leqslant 0.1$. As we shall see later on, this criterion is indeed satisfied for volatile liquid chemical releases of practical interest. It is worth noting that observations of smoke plumes from a large power station suggest the sudden transition assumed here, from jet momentum driven entrainment to a wind dispersion[17].

In the present model, the ground-level dispersion is handled in the same way as the elevated dispersion, except that the momentum equations, Equations (13) and (15), and kinematic equations, Equations (18) and (19), are replaced by corresponding equations that account for gravity compaction and sideways spreading. For simplicity we adopt the SLAB model (Morgan *et al.*[2]) and assume that the cross-section of the ground-level jet is rectangular, with height $2z$ and radius (half-width) R. Note that z still represents the vertical distance from the ground to the centreline of the jet. Beyond ground contact, Equation (23) for the perimeter of the jet is replaced by the expression

$$C = 4z + A/(2z) \tag{30}$$

This relation for the rectangular jet is derived by not allowing entrainment to occur at the jet-ground interface. The half-width of the jet R at ground contact is calculated by setting the perimeter and area of the rectangular ground-level jet equal to those of the circular elevated jet. This ensures that in the post-ground contact region the masses within the jet are conserved and that the continuity and smoothness of concentrations- and temperature-with-distance are preserved. A discontinuity in R will exist at ground contact.

The momentum equation applied to the side edges of the jet is

$$\frac{d}{ds}(\rho A u v) = g(\rho - \rho_\infty)(2z)^2 \tag{31}$$

where v is the velocity of the jet in the lateral direction (or the spreading rate). The momentum equation in the axial direction is

$$\frac{d}{ds}(\rho A u^2) = W\frac{d}{ds}(\rho A u) - g\frac{d}{ds}[(\rho - \rho_\infty)Az] \tag{32}$$

After jet touchdown, these equations are substituted for Equations (13) and (15). The motion of the material interface represented by a side edge of the jet is given by the kinematic condition

$$u\frac{dR}{ds} = v_{en} + v \tag{33}$$

where v_{en} and v are the velocities normal to the edge. With the aid of the equation for the cross-sectional area of the plume, namely $A = 4zR$, Equation (33) can be written as follows

$$\frac{dz}{ds} = \frac{z}{A}\frac{dA}{ds} - \frac{4z^2}{A}\left(\frac{v_{en} + v}{u}\right) \tag{34}$$

which replaces Equation (18) after plume touchdown. Finally, during the gravity spread calculation, Equation (19) takes the form

$$\frac{dx}{ds} = 1 \quad \text{(i.e. } \theta = 0\text{)} \tag{35}$$

It should be mentioned that the only new variable that appears after the transition is made from the airborne plume to the ground-level dispersion is the spreading velocity v; it is assigned the initial condition $v = 0$ at the location of ground contact.

From this system of equations we can compute the jet temperature, released species and entrained water concentrations, jet boundaries, jet velocity, etc. as a function of distance from the source. To utilize available computer subroutines, the equations were converted to an equivalent coupled system of first-order ordinary differential equations by expanding the derivatives in Equations (9)–(11), (13), (15), (16), (31), and (32). Numerical integration was performed using a library program based on the Gear[18] method (see also Hindmarsh[19]).

Comparison of model results with field test data

The tests whose results we have used for model comparisons are: Desert Tortoise (DT) 4 liquid ammonia (NH_3) release; Goldfish (GF) 1 and 3 liquid anhydrous hydrofluoric acid (HF) release; and Energy Analysts' (EA) 1 and 2 small-scale liquid ammonia and propane releases. The choice of these tests is based on the availability of good experimental data. The test parameters are shown in *Table 1*. Additional test details can be found in the references cited below. It should be noted from the table that the liquids were released in the direction of the wind approximately 1 m above ground level as a horizontal jet ($\theta_0 = 0$). The only exception was EA ammonia test 1 where the release angle from the horizontal $\theta_0 = 10°$. Thus in most of the tests the jet made contact with the ground a short distance downwind from the source. The release heights were not reported for the Goldfish series of tests. For the purpose of carrying out HF dispersion calculations, a release height $z_0 = 0.79$ m was assumed. Ammonia was released from this height during the Desert Tortoise series of tests, which were conducted at the same test site as the Goldfish tests.

The Desert Tortoise series test results were reported by Goldwire *et al.*[20] and Goldwire[21]. In *Figure 2*, the predicted profile for the DT4 ammonia plume is presented out to 300 m from the source. Water droplet formation is predicted to occur essentially at the source. The jet is predicted to impact the ground at 2.92 m downwind from the source. Goldwire *et al.*[17] reported that a noticeable pool of liquid ammonia persisted within at least 3 m of the source. The liquid ammonia and water aerosols are predicted to evaporate completely at 40.7 and 201 m downwind, respectively. The actual plume was visible to a point approximately 400 m downwind, indicating, perhaps an overprediction of the entrainment rate. The calculation suggests that the atmospheric water content is responsible for long range visibility of the plume and not the liquid ammonia.

In *Figure 3*, the predicted plume boundaries are superimposed on the measured ammonia concentration contours for two crosswind planes, at 100 m and 800 m downwind from the release. The comparison indicates fair agreement, although the predicted jet cross-section at 800 m is somewhat higher than the experimental data.

The temperature and ammonia concentrations versus distance from the source are compared in *Figures 4* and *5*. The predicted quantities represent average values, while the experimental data for the temperature in the far field and the concentration are the measured values close to the centre of the jet at an elevation of 1 m. The temperature measurements in the near field, at the 3, 6, and 9 m locations, represent those of the liquid ammonia deposited on the ground just downwind of the source. As seen in *Figure 4*, the model is in excellent agreement with the measured temperatures in the near and far field. The model performance in the far field, however, may not be as

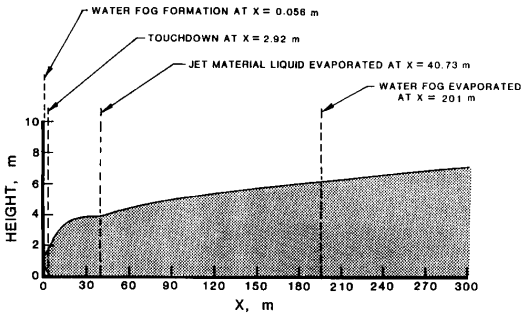

Figure 2 Predicted jet profile for Desert Tortoise ammonia spill Test 4 (DT4)

Table 1 Experimental conditions for field tests

Test	Ref.	Liquid	$T_{js}(P_\infty)$ (K)	P_0 (MPa)	T_0 (K)	T_∞ (K)	RH (%)	A_b (m^2)	z_0 (m)	θ_0	W ($m\ s^{-1}$)
DT4	20,21	NH_3	240	1.4	297	306	21.0	7×10^{-3}	0.79	0	4.5
GF1	26	HF	293	0.87	313	310	5.1	1.4×10^{-3}	—	0	5.6
GF3	26	HF	293	0.91	312	300	27.9	4.6×10^{-4}	—	0	5.4
EA1	27	NH_3	240	0.83	292	292	49.0	3.4×10^{-4}	1.22	10	7.62
EA2	27	C_3H_8	231	1.03	289	289	51.0	1.05×10^{-4}	0.8	0	5.08

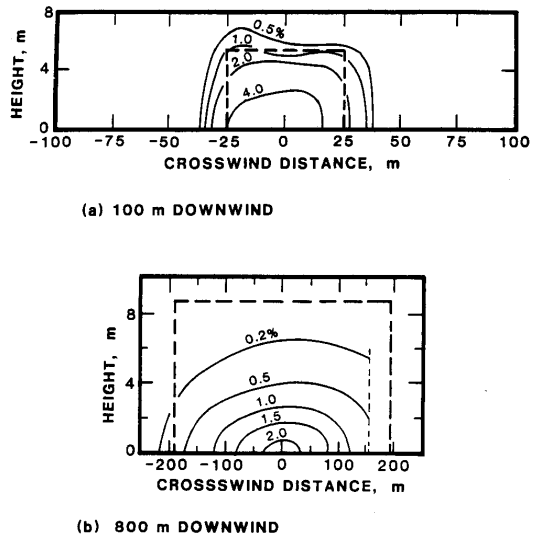

Figure 3 Predicted crosswind jet dimensions (– – –) superimposed on measured ammonia concentrations for Desert Tortoise spill Test 4 (DT4). The predicted average concentrations for the a, 100 m; and b, 800 m downwind locations are 6.5% and 0.92%, respectively.

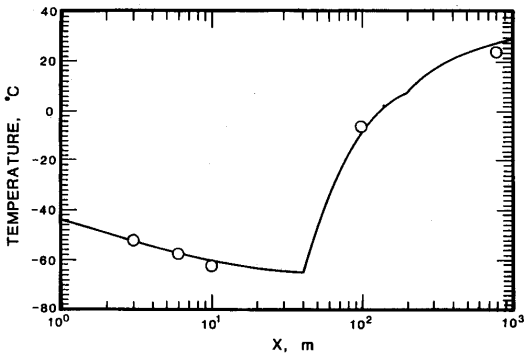

Figure 4 Temperature as a function of distance from source for Desert Tortoise ammonia Test 4 (DT4). The temperature measurements (○) at the 3, 6, and 9 m locations are those of the liquid ammonia deposited on the ground. The open points at 10^2 and 10^3 m downwind are measurements of the jet centreline temperature at 1 m height. The predicted curve is crosswind averaged values

good as the figure suggests, since the model predicts the average temperatures while the measurements correspond to jet centreline values at an elevation of 1 m. In *Figure 5*, the model is seen to predict the ammonia concentration at the 100 m position and underpredict the concentrations at the 800 and 1000 m positions by factors of 2.0 and 3.0, respectively (see also *Table 2*). This level of accuracy is considered to be reasonable in the field of modelling the dilution of chemical releases in the atmosphere[5]. Again, the model results are average values, while the experimental data are the measured values at the centre of the jet.

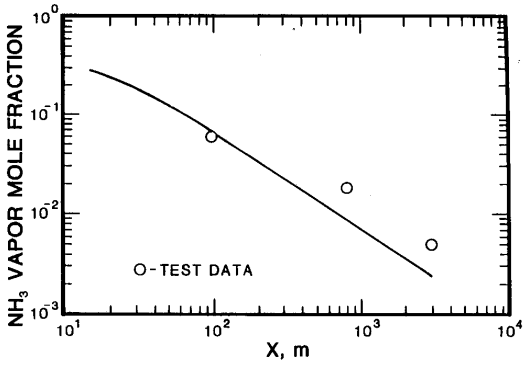

Figure 5 Ammonia concentration as a function of distance from source for Desert Tortoise spill Test 4 (DT4): ○, measurements of the centreline concentration at an elevation of 1 m. The predicted curve is crosswind averaged values

Table 2 Comparison of theory with concentration measurements

Distance downwind (m)	Concentration (mole fraction)[a]			
	DT4		GF3	
	Measurement	Prediction	Measurement	Prediction
100	6×10^{-2}	6.5×10^{-2}	—	—
300	—	—	9.5×10^{-3}	1.0×10^{-2}
800	2×10^{-2}	9.2×10^{-3}	—	—
1000	—	—	1.3×10^{-3}	1.5×10^{-3}
3000	5×10^{-3}	1.6×10^{-3}	1.8×10^{-4}	2.9×10^{-4}

[a]Measured values at jet centreline 1 m above ground; predictions are crosswind averaged values

Interestingly enough, the entrainment velocity v_{en} given by Equation (8) did not fall below v_{en} given by Equation (28) during the course of the calculation that produced the NH_3 concentration versus distance curve of *Figure 5*. Thus for a distance downwind of the source of at least 3000 m, it does not appear to be necessary to invoke the presence of atmospheric turbulence due to wind to explain the measured NH_3 jet dilution. While at first sight this result may seem surprising, it should be mentioned that many other examples have been reported in the literature in which self-generated turbulence dominates the jet mixing process far downstream of the source. Briggs[22] compiled data which show that Equation (8), with $E_1 = 0$ and $E_0 \approx 0.1$, can be applied to plumes extending 3000 m above an oil fire (see also Turner[23]). The distance range over which Equation (8) is valid was extended by another order of magnitude: Wilson *et al.*[24] and later on Sparks[25] successfully applied the formula to describe plumes of hot gas emitted from erupting volcanoes. Such plumes reach heights greater than 40 000 m. Slawson and Csanadys'[17] observations of smoke plumes released from a power plant stack into a cross-wind showed that the transition from plume-to-atmospheric generated

entrainment occurs at distances as large as 425 m from the chimney. Hoult *et al.*[13] have applied an entrainment formula similar to Equation (8) to explain data collected on chimney plumes in a cross-wind and found the formula to be valid over a distance of approximately 1800 m from the chimney. Note that in such chimney plumes only buoyancy is responsible for plume momentum at the source, yet self-generated turbulence dominates the entrainment process far downstream from the chimney. Finally, with regard to the DT4 NH_3 release simulation, it is significant to note that the predicted Richardson number is 0.02 at the source, rises to a maximum value of 0.11 at about 200 m downwind and then decays to zero in the very far field. Clearly, for high-momentum jets, gravity is not an important feature of the entrainment process.

The hydrogen fluoride dispersion experiments were conducted and reported by Blewitt *et al.*[26]. The liquid HF and atmospheric water condensate for Test GF1 are predicted to evaporate in the near field, at approximately 24 and 29 m, respectively. During GF1 the jet was visible to a distance of approximately 700 m from the source. Thus the visibility of the jet in the far field cannot be explained by the presence of water droplets alone. Hydrogen fluoride and water vapour exhibit a strong chemical interaction which results in the formation of a condensed phase (aerosol) of HF/H_2O solution droplets. These relatively stable, chemically produced droplets would be expected to persist out to significant distances from the source. The present model is based entirely on consideration of local phase-change thermodynamic equilibrium. Chemical reactions between the jet material and water vapour are not considered. The measured centreline temperatures and HF concentrations for Tests GF1 and GF3 were found to agree well with the cross-wind averaged values of the model. The measured and predicted temperature and concentration versus distance curves for Test GF3 are shown in *Figures 6* and *7*, respectively. The numerical solutions indicate that the application of an entrainment equation for high-

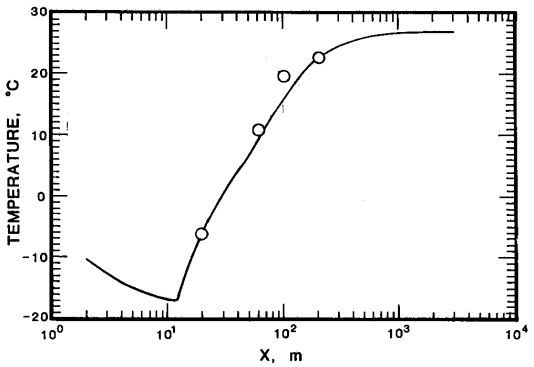

Figure 6 Temperature as a function of distance from source for Goldfish hydrofluoric acid spill Test 3 (GF3): ○, measurements of the jet centreline temperature at 1 m height. The predicted curve is crosswind averaged values

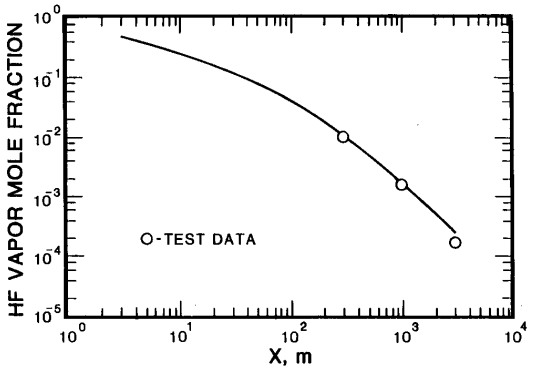

Figure 7 Hydrofluoric acid concentration as a function of distance from the source for Goldfish hydrofluoric acid spill Test 3 (GF3): ○, measurements of the jet centreline concentration at an elevation of 1 m; solid curve, crosswind averaged values

momentum jets, namely Equation (8), is not valid for distances from the source beyond about 80 m for the HF tests. At this point the transition is made between high-momentum jet and Gaussian plume entrainment behaviour. Neglecting entrainment associated with atmospheric turbulence will lead to over-estimates of the concentration. The predicted maximum Richardson number for both tests is only about 0.02 at about 10 m from the source, indicating once again that buoyancy does not influence the entrainment process in an essential way.

Note from *Table 1* that the break area and stagnation pressure for the NH_3 test are much larger than the corresponding quantities for the HF tests. This readily explains why the NH_3 jet in Test DT4 was dominated by the momentum flux from the source at all the concentration sampler stations, while the momentum flux for the weaker (Test GF3) HF jet vanished some distance upwind of the first concentration sampler, and beyond this point spreading was dominated by atmospheric turbulence.

Small-scale field releases of pressurized liquid ammonia and propane were performed by Pfenning *et al.*[27] (the Energy Analysts (EA) series). Using slides and video tapes, the average profile of the visible portion of the jet was obtained. No vapour concentration or temperature measurements were made. In Test EA1 (see *Table 1*) the liquid ammonia was released at a 10° incline from the horizontal. *Figure 8* shows the predicted profile of the ammonia jet for Test EA1. The visible jet extended approximately 45 m downwind, with a maximum height of 3.7 m. This is to be compared with the prediction of 40.4 m, based on complete water droplet evaporation, and the predicted maximum height of 3.9 m. The predicted length of the visible propane jet for Test EA2 is 17.9 m and the predicted maximum jet height is 1.9 m. The visible length and maximum jet height measured were 24 m and 2.1 m, respectively. In both the EA1 and EA2 releases the jet material aerosol is predicted to evaporate completely before contact with the ground. This is

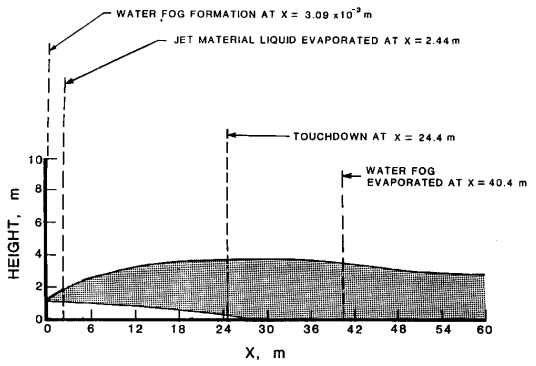

Figure 8 Predicted jet profile for Energy Analysts' ammonia release test (EA1)

consistent with the observations of Pfenning *et al.*[27] that in the tests no liquid accumulated on the ground.

Validity of aerosol generation model

Of the three jet spreading models that comprise the present composite model of the dilution of a two-phase chemical plume, the Gaussian plume model and, as pointed out in the previous section, the high-momentum jet dispersion model are frequently used and accepted in the literature on dispersion modelling in the atmosphere (or hydrosphere). Thus we will focus our attention on the validity of the jet depressurization and aerosol formation model, namely Equations (1) through (7), which represents a new addition to the theory of dispersion modelling.

One of the principle assumptions of the theory presented here is that during depressurization the released liquid disintegrates into fine droplets by flashing. From the laboratory studies of Brown and York[28] and Gooderum and Bushnell[29] it is known that the range of drop sizes achieved by flashing liquid jets is 10–50μm. The local differences in temperature and velocity between the vapour and such small aerosol droplets are negligible. Thus thermodynamic equilibrium and overall momentum balance calculations are sufficient to determine the flow rates of the phases formed and the expanded jet diameter at the end of depressurization zone; it is not necessary to determine the droplet size distribution.

Of course, there is a threshold temperature below which the jets will not shatter into fine droplets. Bushnell and Gooderum[30] measured the flashing or shatter temperature of superheated water jets under conditions where the aerodynamic forces are of secondary importance (i.e. at low Weber numbers in a low pressure environment). Their data show that the amount of superheat that can be tolerated by a single-phase orifice flow of water is given by the equation

$$N = \frac{T_{sh} - T_s}{T_{sh}} \approx 0.1 \qquad (36)$$

where T_{sh} and T_s are the shatter and saturation temperatures, respectively. Earlier work by Brown and York[28] is consistent with this upper bound on liquid superheat. However, a careful examination of the data of both Bushnell and Gooderum[30] and Brown and York[28] indicates that, in practice, the actual shatter temperature will fall below the maximum value corresponding to $N = 0.1$, owing to Weber number effects, vaporization upstream of the orifice, and the roughness of the injector.

All the field data reported in Refs. 20, 21, 26, 27 correspond to an observed high degree of dispersion of the liquid, and in most cases the value of N exceeded 0.1. However, the shattering of HF jet releases[26] occurred for $N = 0.065$. The near explosive generation of vapour and aerosol is not restricted to a particular superheat value because flashing is a nucleation event which depends very much on the foreign nuclei that are present in the liquid. Suitable nuclei are: dissolved gas, suspended dust or debris, and low pressure eddies caused by orifice surface roughness or Weber number effects. These nucleation effects are very difficult to characterize and, therefore, it would be difficult to further narrow the already narrow temperature range between the liquid boiling point (at one atmosphere) and observed jet disintegration. For example, in the case of water jets released into the atmosphere[28], the minimum observed value of $N = 0.03$ is equivalent to a liquid superheat necessary for flash evaporation of only 11 °C. Realistically, considering all the uncertainties associated with an emergency release, any attempt to distinguish between such a small superheat and zero superheat is unwarranted. The only sensible and conservative approach is to assume that the liquid release is shattered into fine droplets if it is heated above its boiling point.

Finally, it should be mentioned that the jet depressurization model employed here has been successfully used to predict thrust and jet impingement forces which accompany vessel 'blowdown' events[31,32]. The fact that predicted jet impingement forces give reasonable agreement with water blowdown data indicates that the model correctly estimates the fully expanded asymptotic jet properties. In this regard, it is of interest to note that Waitkus and Griffiths[33] measured the velocity of a flashing phenol/formaldehyde release just outside the vent. The present depressurization model predicts a fully expanded jet velocity of 45.7 m s^{-1}. The observed velocity of the phenol/formaldehyde aerosol was 39.6 m s^{-1}.

Conclusions

In this paper we have provided a modelling approach to determining the dispersion hazards arising from the release of pressurized liquid chemicals. The dilution of the two-phase jet produced by the release has been modelled taking into account the three regimes of jet behaviour. A one-dimensional source model describing the depressurization of the jet and two turbulent

entrainment models describing the elevated and ground-level behaviour have been presented.

The comparison of field observations of jet temperature and dilution with the theory shows that the predictions can reproduce the NH_3 data within a factor of three. Within the limits of the observations, which were made for distances downwind of the source of less than 3000 m, there appears to be no necessity of involving the presence of atmospheric turbulence due to wind to explain the measured NH_3 jet dilution. The value of the entrainment parameter $E_0 = 0.1$, which produces reasonable agreement between the field observations and the theoretical calculations, falls within the range of values $E_0 = 0.05–0.12$ which gives the best agreement between theory and laboratory model experiments on entrainment by turbulent gas jets. For the two selected HF release experiments, the model was observed to predict a transition from the high-momentum regime to the atmospheric turbulence regime of jet dilution at about 80 m downwind of the source. The model is in good agreement with the measured HF concentrations over the entire 3000 m sampling distance. The difference in entrainment behaviour between the NH_3 and HF jets can be attributed to the much larger momentum associated with the NH_3 test compared with that for the HF tests.

References

1 Morton, B. R., Taylor, G. I., and Turner, J. S. *Proc. Royal Society London, Ser. A* 1956, **234**, 1
2 Morgan Jr., D. L., Morris L. K. and Ermak, D. L., 'SLAB: A Time-Dependent Computer Model for the Dispersion of Heavy Gases Released in the Atmosphere', Lawrence Livermore National Laboratory Report UCRL-53383, 1983
3 Chan, S. T., 'FEM3 – A Finite Element Model for the Simulation of Heavy Gas Dispersion and Incompressible Flow: User's Manual', Lawrence Livermore National Laboratory Report UCRL-53397, 1983
4 Havens, J. A. and Spicer, T. O., 'Development of an Atmospheric Dispersion Model for Heavier-than-Air Gas Mixtures', Final Report to U.S. Coast Guard, Contract DT-CG-23-80-C-20029, May 1985
5 Blewitt, D. N., Yohn, J. F., and Ermak, D. L., 'An evaluation of SLAB and DEGADIS Heavy Gas Dispersion Models Using the HF Spill Test Data', in International Conference on Vapor Cloud Modelling, 2–4 November 1987, Cambridge, Massachusetts, USA, (Ed. J. Woodward), pp. 56–80
6 Chan, S. T., Rodean, H. C., and Blewitt, D. N., 'FEM-3 Modeling of Ammonia and Hydrofluoric Acid Dispersion', in International Conference on Vapor Cloud Modeling, 2–4 November 1987, Cambridge, Massachusetts, USA, (Ed. J. Woodward), pp. 116–154
7 Spicer, T. O. and Havens, J. A., 'Modeling HF and NH_3 Spill Test Data Using DEGADIS', AIChE Summer National Meeting, Paper No. 87b, August 1988
8 Fauske, H. K. and Epstein, M. *J. Loss Prev. Process Ind.* 1988, **1**, 75
9 Gebhart, B., Hilder, D. S., and Kelleher, M., in 'Advances in Heat Transfer', (Eds. J. P. Hartnett, and T. F. Irvine,) 1984, **16**, 1
10 Hirst, E. A., 'Analysis of Round, Turbulent, Buoyant Jets Discharged to Flowing Stratified Ambients', Oak Ridge National Laboratory Report ORNL-4685, 1971
11 Ricou, F. B. and Spalding, D. B. *J. Fluid Mechanics* 1961, **11**, 21
12 Morton, B. R. *J. Fluid Mechanics* 1959, **5**, 151
13 Hoult, D. P., Fay, J. A., and Forney, L. J. *J. Air Pollution Control Assoc.* 1969, **19**, 585
14 Seinfeld, J. H., in 'Atmospheric Chemistry and Physics of Air Pollution', John Wiley & Sons, New York, USA, 1986
15 Burgess, D., Murphy, J. N., Zabetakis, M. G., and Perlee, H. E., 'Volume of Flammable Mixture Resulting from the Atmospheric Dispersion of a Leak or Spill', 15th International Symposium on Combustion, 1974, pp. 289–303
16 Ellison, T. H. and Turner, J. C. *J. Fluid Mech.* 1959, **6**, 423
17 Slawson, P. R. and Csanady *J. Fluid Mech.* 1967, **28**, 311
18 Gear, C. W., in 'Numerical Initial Value Problems in Ordinary Differential Equations', Prentice Hall, Englewood Cliffs, New Jersey, USA, 1971
19 Hindmarsh, A. C., 'Linear Multistep Methods for Ordinary Differential Equations: Method Formulations, Stability, and the Methods of Nordsieck and Gear', Lawrence Livermore National Laboratory Report UCRL-51185, Rev. 1, March 1972
20 Goldwire Jr., H. C., McRae, T. G., Johnson, G. W., Hipple, D. L. *et al.* 'Desert Tortoise Series Data Report – 1983 Pressurized Ammonia Spills', Lawrence Livermore National Laboratories Report UCID-20562, December 1985
21 Goldwire Jr., H. C. *Chem. Eng. Prog.* 1986, April, 35
22 Briggs, G. A. in 'Plume Rise', US Atomic Energy Commission Critical Review Series, 1969
23 Turner, J. S., in 'Buoyancy Effects in Fluids', Cambridge University Press, UK, 1973
24 Wilson, L., Sparks, R. S. J., Huang, T. C., and Watkins, N. D. *J. Geophysical Research* 1978, **83**, 1829
25 Sparks, R. S. J. *Bulletin Volcanol.* 1986, **48**, 3
26 Blewitt, D. N., Yohn, J. F., Koopman, R. P. and Brown, T. C., 'Conduct of Anhydrous Hydrofluoric Acid Spill Experiments', in International Conference on Vapor Cloud Modeling, 2–4 November 1987, Cambridge, Massachusetts, USA, (Ed. J. Woodward), pp. 1–38
27 Pfenning, D. B., Millsap, S. B., and Johnson, D. W., 'Comparison of Turbulent Jet Model Predictions with Small-Scale Pressurized Releases of Ammonia and Propane', in International Conference on Vapor Cloud Modeling, 2–4 November 1987, Cambridge, Massachusetts, USA, (Ed. J. Woodward), pp. 81–115
28 Brown, R. and York, J. L. *AIChE Journal* 1962, **8**,149
29 Gooderum, P. B. and Bushnell, D. M. *J. Spacecraft and Rockets* 1969, **6**, 197
30 Bushnell, D. M. and Gooderum, P. B. *J. Spacecraft and Rockets* 1968, **5**, 231
31 Moody, F. J., 'Prediction of Blowdown Thrust and Jet Forces', Paper presented at ASME-AIChE Heat Transfer Conference, Minneapolis, Minnesota, August 1969, ASME Paper 69-HT-31
32 Epstein, M., Henry, R. E., Midvidy, W., and Pauls, R. E., in 'Thermal-Hydraulics of Nuclear Reactors', Vol. II, 2nd Topical Meeting on Nuclear Reactor Thermal-Hydraulics, 11–14 January 1983, Santa Barbara, California, USA
33 Waitkus, P. A. and Griffiths, G. R., 'Explosion Venting of Phenolic Reactors – Toward Understanding Optimum Explosion Vent Diameters', Society of Plastics Engineers, National Technical Conference, Denver, Colorado, USA, 8–10 November 1977, pp. 181–186

Nomenclature

A	cross-sectional area of plume
A_b	area of vent or rupture opening
A_e	area of jet at end of depressurization zone
$c_{j,f}$	heat capacity of liquid jet material
C	circumference of plume through which entrainment occurs
C_D	vent or rupture opening discharge coefficient
E_0, E_1	entrainment constants, see Equation (8)
g	gravitational acceleration
G	choked mass flux release rate, see Equation (1)
h	enthalpy (unsubscripted symbol pertains to the mean plume enthalpy)
P	pressure
R	radius of circular plume or half-width of rectangular plume, or ideal gas constant (with subscript)
Ri	Richardson number, see Equation (29)
s	distance measured from the source along plume centreline
T	temperature
u	mean velocity inside plume
u_e	velocity of jet at end of depressurization region
v	spreading velocity of plume
v_{en}	entrainment velocity

W	velocity of wind	a	air
x	distance measured from the source along the ground	e	at end of depressurization zone
x_e	quality of jet at end of depressurization zone	f	liquid phase
z	distance measured from ground to plume centreline	fg	liquid–gas phase transition
		g	gas phase
ρ	density (unsubscripted symbol pertains to the mean plume density)	j	jet or plume material release
		o	stagnation or vessel condition
ρ_∞	density of the humidified atmosphere	s	saturated or equilibrium state
σ_y, σ_z	Gaussian dispersion coefficients in y- and z- directions	w	water
θ	angle of plume centreline with horizontal	∞	pertains to the atmosphere